Radiative Transfer through Broken Clouds: Observations and Model Validation

DANA E. LANE,* KRISTEN GORIS, AND RICHARD C. J. SOMERVILLE

Climate Research Division, Scripps Institution of Oceanography, University of California, San Diego, La Jolla, California

(Manuscript received 23 January 2001, in final form 16 April 2002)

ABSTRACT

Stochastic radiative transfer is investigated as a method of improving shortwave cloud–radiation parameterizations by incorporating the effects of statistically determined cloud-size and cloud-spacing distributions. Ground-based observations from 16 days at the Atmospheric Radiation Measurement (ARM) Program's Southern Great Plains (SGP) site are used to derive a statistical description of scattered clouds. The data are ingested into a stochastic, shortwave radiative transfer model. The typical cloud-base height of the most prevalent cloud type, fair-weather cumulus, is 1100 m. Low cloud-fraction conditions are common, with observed cloud liquid water paths between 20 and 80 g m^{-2}. Cloud-fraction amounts calculated using ceilometer data compare reasonably well with those reported in weather logs. The frequency distribution of cloud size can be described by a decaying exponential: the number of clouds decreases significantly with increasing cloud size. The minimum detectable cloud size is 200 m and the largest observed cloud is approximately 4 km. Using both a stochastic model and a plane-parallel model, the predicted radiation fields are compared and evaluated against an independent observational dataset. The stochastic model is sensitive to input cloud fraction and cloud field geometry. This model performs poorly when clouds are present in adjacent model layers due to random overlapping of the clouds. Typically, the models agree within 30 W m^{-2} for downwelling shortwave radiation at the surface. Improvement in the observations used to calculate optical depth will be necessary to realize fully the potential of the stochastic technique.

1. Introduction

The representation of clouds in atmospheric general circulation models (AGCMs) has been shown to be a major cause of climate prediction uncertainty (Senior and Mitchell 1993; Houghton et al. 1996). Several studies have shown that oversimplification of cloud macroscopic properties such as size, shape, and spatial distribution results in significant error in model predictions of cloud radiative forcing (e.g., Cahalan et al. 1994; Ellingson 1982; Kite 1987; Welch and Wielicki 1984; McKee and Klehr 1978). Incorporating information about cloud scale and spatial distribution into cloud and radiation modeling has long been recognized as an important step toward an improved understanding of atmospheric radiative transfer (e.g., Plank 1969; Kuhn 1978; Stephens and Platt 1987). A statistical representation of the cloud field such as that used in stochastic theory may be a useful approach to modeling broken or scattered clouds (Stephens 1988; Malvagi and Pomraning 1993). However, these statistical models require specific geometrical and physical information about the cloud field that has been unavailable until recently.

In this study, a novel method for deriving cloud spatial and physical properties from ground-based observations made at the Atmospheric Radiation Measurement Program (ARM; Stokes and Schwartz 1994) Clouds and Radiation Testbed (CART) is used to provide cloud field characteristics. These measurements can be analyzed to create input for a stochastic radiative transfer model. Low-level, scattered cumuli, which are difficult to represent in AGCMs, are selected for this case study. Data from weather observation logs, cloud observation platforms, and other ground-based instruments are used to determine optical and geometrical characteristics for each analyzed cloud type. Results include frequency distributions of cloud-base height, cloud-top height, cloud fraction, liquid water path, cloud horizontal scale, and cloud spacing for each cloud type. All fields are analyzed in a manner that yields information appropriate for input to the stochastic radiative transfer model.

2. Model description

a. Stochastic model

The stochastic model employed in this study was developed by Somerville, Byrne, Malvagi, Pomraning,

* Current affiliation: Department of Environmental Sciences, Rutgers–The State University of New Jersey, New Brunswick, New Jersey.

Corresponding author address: Dana E. Lane, Department of Environmental Sciences, Rutgers–The State University of New Jersey, 14 College Farm Road, New Brunswick, NJ 08901.
E-mail: lane@envsci.rutgers.edu

and Subasilar (Byrne et al. 1996; Malvagi et al. 1993; Malvagi and Pomraning 1993), and was derived from linear kinetic theory (Pomraning 1991). It has been modified for this study to incorporate realistic cloud fields (Lane and Somerville 2002, manuscript submitted to *J. Geophys. Res.*, hereafter LS). The stochastic model contains 38 shortwave and near-infrared radiation bands that range from 2500 to 50 000 cm^{-1}. In each band there are two possible absorbers, of which water vapor is often one. The model atmosphere is taken from climatological McClatchey (1972) profiles for the continental midlatitude summer. There are 32 standard pressure layers, and a horizontal domain equivalent to that of an AGCM grid box. The stochastic model assumes that the cloudy atmosphere is composed of two materials: cloud and clear sky. The clouds do not contain internal variability, and are distributed in the clear sky using Markovian (exponential) statistics. These statistics are appropriate when the size of the horizontal domain is much larger than the size of individual clouds (Malvagi and Pomraning 1993). This situation is interesting because clouds may function as light sources for each other (Byrne et al. 1996). Therefore, a photon may exit and enter several different clouds before reaching the surface, being absorbed, or returning to space.

The stochastic model utilizes several input parameters. This includes cloud-base and cloud-top height, total cloud water path, effective radius, and cloud fraction. Additionally, the appropriate solar angle must be supplied to the model. The stochastic model also requires the characteristic horizontal scale of the clouds. This input is unique to the stochastic approach to modeling cloud–radiation interactions, and is an improvement to the realism of the model cloud field. The stochastic model represents this geometrical influence as gain/loss terms that are included in the radiative transfer equation. These terms indicate the contribution of photons that transited from one material to another (clear to cloud or cloud to clear) in a time step. Each gain/loss term is weighted by a probability function that is derived from the fractional cloud cover, cloud field geometry, and linear kinetic theory. The clouds are assumed to be ellipsoidal in shape.

All clouds in this study are represented as liquid clouds. The cloud horizontal scale, thickness, and optical properties are used to derive a probability distribution of volume extinction coefficients that is defined as Markovian. Then the radiative transfer equation is solved iteratively over the distribution using a discrete-ordinates technique. The cloud fraction is used to appropriately weight the new gain and loss terms in the radiative transfer equations. In previous studies of the stochastic approach, most of the inputs were theoretically determined. In this study, the input quantities are derived from observations from the ARM Program's Southern Great Plains (SGP) site and ingested by the stochastic model on an hourly basis.

The output of the stochastic model is the domain-averaged transmitted, absorbed, and reflected shortwave radiation (by band) at each atmospheric layer as well as the calculated clear- and cloudy-sky pathlengths. Predictions of the radiation fields are performed using eight scattering angles. For these simulations, the broadband, domain-averaged downwelling shortwave radiation will be compared to that predicted by the plane-parallel model and to observations. A distinct advantage of this approach is that a stochastic model can accurately calculate the radiative heating rates through a broken cloud layer without requiring an exact description of the cloud geometry.

b. Plane-parallel model

The radiative transfer model used for comparison is typical of the shortwave cloud–radiation routines utilized in current AGCMs. The model, SUNRAY, was developed by Fouquart and Bonnel (1980), and has two spectral bands, one in the shortwave part of the spectrum (0.25–0.68 μm) and one in the near-infrared part of the spectrum (0.68–4.00 μm). There are 30 atmospheric layers, the characteristics of which have been adjusted to match those in the stochastic model. The plane-parallel model cannot specify cloud field geometry beyond a cloud fraction. Therefore, all clouds in these simulations are confined to one layer, the second pressure layer from the surface, which approximates the observed cloud height. The inputs to the plane-parallel model are cloud optical thickness and cloud fraction. Optical thickness is calculated from the observed cloud liquid water path following Liou (1992). The model performs one clear-sky calculation and one overcast calculation. The resulting radiative terms are combined in a sum weighted by fractional cloud coverage. The model outputs the two-stream shortwave radiative flux at each level.

3. Development of input parameters

To determine whether the stochastic approach to cloud–radiation modeling is appropriate for actual cloud and radiation fields, observational data must be used to derive the necessary input. As in most cloud–radiation codes, cloud optical properties are needed, as well as information about the cloud height and fractional coverage. Particular to this approach, cloud-size and cloud-spacing statistics must be determined observationally. This has been done to some extent with aircraft and satellite studies (e.g., Plank 1969; Hozumi et al. 1982; Welch and Wielicki 1984). The ARM SGP site consists of a large area covering parts of Oklahoma and Kansas and is similar in size to an AGCM grid cell. The site provides continuous, ground-based cloud and radiometric observations to the scientific community with the specific focus on improving cloud–radiation parameterizations. These measurements can provide the cloud optical and geometric properties required by the stochastic

TABLE 1. Cloud-type identification key and size of dataset.

Cloud type	Category	Description	No. hours in dataset
1	Detached masses	Small with slight vertical development (typical fair-weather type)	24
4		Spread out from cumulus without vertical development	6
8	Sheet or layer	Stratocumulus with towering cumulus below or with cumulus or cumulonimbus penetrating the layer	15

model. Most of the instruments used in this study were located at the central facility of the SGP CART site.

As mentioned in the stochastic model description, this approach is only appropriate under certain situations. Therefore, several hours of data from 1998 were selected using strict criteria that attempted to isolate appropriate geometrical circumstances. Initially, hourly meteorological logs recorded by human observers during daylight hours were analyzed to identify the occurrence of broken, low-level clouds. Selected days were required to have at least two consecutive hours of broken clouds. Clouds with base heights greater than 2 km were not considered. This apparently arbitrary limit arose from using the Multifilter Rotating Shadowband Radiometer (MFRSR) to distinguish individual clouds. The presence of multiple cloud types or cloud layers disqualified much of the observational dataset. Finally, times with smoke or dust from farming were removed to avoid the influence of heavy low-level aerosol on the calculation of optical depth. Altogether, 45 h (16 days) were selected that met the above criteria, in the period from January to December 1998.

The dataset is partitioned by cloud type, which is recorded in an hourly meteorological log, along with cloud-base height and cloud fraction. There are three cloud types included in this study, identified as type-1, type-4, and type-8 clouds. This corresponds to the World Meteorological Office designations of C_L1, C_L4, and C_L8 (World Meteorological Organization 1956). In this article, we focus on type-1 clouds, which are fair-weather cumulus and cumulus fractus clouds. As the cloud optical and geometrical properties are discussed, variations of the two other types from type 1 will be noted. For descriptions of the individual cloud types and the number of hours per type in the dataset, refer to Table 1. Type-1 clouds generally occur at the top of boundary layer thermals. They usually appear flattened and are trapped by a capping inversion (Stull 1991). The lifetime of these low-level cumuli is primarily determined by the mixing rate of in-cloud air with the environment. For fair-weather cumuli, this duration time is approximately 20 min. Type-4 clouds are typically broken stra-

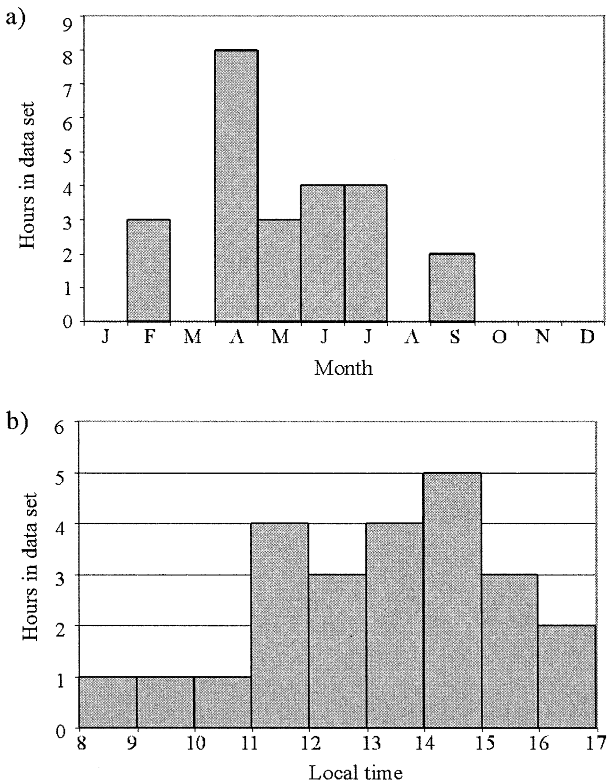

FIG. 1. (a) Yearly distribution of the times of occurrence for type-1 clouds in the dataset. (b) Diurnal distribution of the times of occurrence in the dataset.

tocumulus clouds and type-8 clouds may be developing cumulus congestus.

The cloud-type information was evaluated against images recorded by the Time-Lapsed Cloud Video (TLCV) camera and the Whole Sky Imager (WSI). The TLCV, which records one image every 8 s, allows observation of the evolution of the cloud field. This upward-looking camera has a $100° \times 130°$ field of view and is oriented with the east–west direction along the short axis. The WSI samples at 10-min intervals but has a hemispheric field of view. Both instruments confirm the continuous presence of scattered clouds, however determination of type using the imagers was difficult. Satellite imagery from the *Geostationary Operational Environmental Satellite-8* (*GOES-8*) was used to verify the extent and stability of the cloud field. This is important as the stochastic model assumes that the cloud field is present throughout the domain.

The cloud fields that satisfy the selection criteria for this study at the ARM CART site are found to occur most frequently in the spring and summer. All selected clouds were present during 1600–2400 UTC (Figs. 1a,b), with most clouds occurring between 19 and 22 UTC, again indicating the importance of surface heating. This agrees well with the results of Plank (1969) who observed a maximum in fair-weather cumulus

TABLE 2. Derived cloud field characteristics.

Cloud type	Cloud-base height (m)	Cloud fraction (fraction)	Liquid water path (g m^{-2})	Cloud size (m)	Cloud spacing (m)	Time of occurrence (local time)
1	1100	0.3	50–70	≤300	≤200	Late afternoon
4	700	0.45	20	≤200	≤200	Early afternoon
8	1400	0.2	60–80	≤300	≤300	Early afternoon

cloud amount around 2130 UTC. A summary of the cloud field characteristics can be found in Table 2.

a. *Optical properties*

Optical properties determine most of the impact a cloud has on the radiation fields. As the three cloud types form under different synoptic conditions, it is not surprising that the cloud optical properties are quite different among the three categories. For both models, the cloud liquid water path and effective droplet radius are necessary to characterize the optical depth. It is important to determine both of these inputs as precisely as possible since many shortwave cloud–radiation models are strongly sensitive to these parameters.

1) LIQUID WATER

The liquid water path is derived from vertical line-of-sight observations made by the microwave radiometer (MWR; Taylor and English 1995). The MWR samples microwave radiation in two bands, one of which, the 31.4-GHz channel, is dominated by liquid water in the atmosphere. Brightness temperatures are used to calculate the column water vapor and liquid water path (LWP) using site-specific retrieval coefficients. The initial measurement has large statistical uncertainties (± 30 g m^{-2}), especially for small liquid water amounts. Averaging the observations using a 3-min running mean can reduce this uncertainty to ± 18 g m^{-2} for all cloud types, and ± 5 g m^{-2} for type 1. The average provides a mean cloud water path value for the field, which is appropriate for the hourly model calculations. Measurements of LWP in type-8 clouds have the largest uncertainty. In sensitivity studies performed by the stochastic model, changes of 10 g m^{-2} in LWP caused a change in the downwelling shortwave radiation at the surface of 0–30 W m^{-2} for overcast conditions (LS).

The average LWP values are compiled in hourly histograms per cloud type and summed over the entire dataset (Fig. 2). The probability distribution of liquid water path (Fig. 2) for type-1 clouds is quite wide (20–110 g m^{-2}), with a broad peak in the distribution between 20 and 70 g m^{-2}. The small cumulus clouds observed on the days of this study do not cover a large horizontal area, but cause significant attenuation of the radiation when they pass overhead (Harrison et al. 1994). For type-4 and type-8 clouds, the width of the LWP probability distribution is similar to that shown in Fig. 2. However, the peak in the distribution of LWP is quite narrow and is centered at 20 g m^{-2} for type-4 clouds, while for type-8 clouds the peak is broader and occurs at larger LWP values (60–80 g m^{-2}).

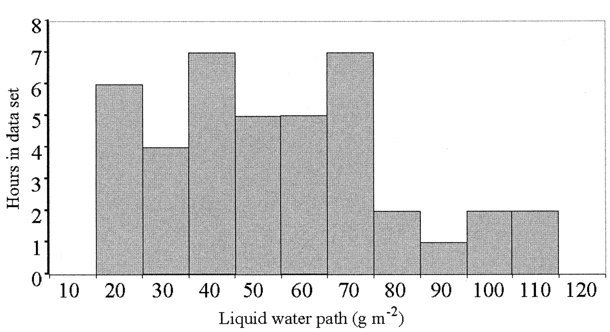

FIG. 2. Distribution of liquid water path.

2) EFFECTIVE RADIUS

The liquid water path derived from the MWR may be used, with an optical depth, to calculate droplet effective radius (R_e) using $R_e \cong 3\,\mathrm{LWP}(2\tau)^{-1}$ (Liou 1992). Here τ is the cloud optical depth and LWP is taken from the MWR measurement. For this purpose, the optical depth is calculated using observations from the MFRSR following Harrison et al. (1994) who employ a straightforward application of the attenuation law $I = I_o e^{-\tau}$, where I_o is the incident intensity and I is the attenuated intensity. This is a determination of the amount the direct beam is attenuated by the clouds, relative to a clear day.

The probability distribution of droplet effective radius resulting from the above technique ranges from 2 to 20 μm for type-1 clouds, with the peak occurring at 9–10 μm (not shown). In comparison with in situ studies of fair-weather cumuli (Stephens and Platt 1987; Battan and Reitan 1957), the width of the derived distribution is acceptable but the peak occurs at an unreasonably high value. Therefore, in the modeling portion of this study a fixed droplet effective radius of 6 μm is used. The selection of this value was based on the climatological value of 7 μm reported by Fenn et al. (1985), and the 4-μm droplet effective radius reported by Battan and Reitan (1957) in their study of fair-weather cumuli over the central United States. A reanalysis of ARM SGP data using millimeter cloud radar data suggests that the typical droplet effective radius for this type of low-level, broken cloud may be 3–4 μm (S. Kato 2000, personal communication). Sensitivity studies with the stochastic model have shown a change of 10–50 W m^{-2} in the downwelling shortwave radiation for a change in effective radius of 1 μm. The greatest sensitivity occurs when LWP is approximately 100 g m^{-2}. Fortunately, most clouds in this study have lower values of LWP.

b. Cloud field geometrical properties

As described above, a benefit of the stochastic approach is that information about the spatial structure of a cloud field can be incorporated in a radiative transfer calculation without specifically modeling individual clouds. Therefore, the geometrical properties of the clouds as well as intercloud spacing are important input quantities. These characteristics will be ingested in the stochastic model as cloud-base height, cloud-top height, cloud horizontal size, and cloud horizontal spacing. The cloud-top and cloud-base height are used to derive cloud depth, which is then combined with the characteristic cloud horizontal scale to approximate the volume the cloud field occupies. This information, combined with the above optical properties, is used by the stochastic model to calculate a volume extinction coefficient.

Several observational studies have characterized the dimensions and spatial distributions of cumulus populations (e.g., Plank 1969; Hozumi et al. 1982; Wielicki and Welch 1986; Joseph and Cahalan 1990; Benner and Curry 1998) using remote sensing methods or in situ photography. Plank (1969) employed aerial photography to study the size distribution of cumulus cloud fields over Florida and found that the cloud number density decreased exponentially with increasing cloud size. Hozumi et al. (1982) report similar cloud distributions using photographic methods comparable to the Plank study. Similarly, Wielicki and Welch (1986), who employed satellite data to study cumulus cloud fields, found similar results for clouds smaller in than 1 km in effective diameter. Joseph and Cahalan (1990) analyzed the nearest neighbor spacing (distance between cloud centers) of cumulus cloud fields using satellite images. They reported cloud spacing to be linearly dependent on cloud size.

1) CLOUD-BASE HEIGHT

At the SGP site, several instruments measure cloud-base height. For this study, the Belfort Laser Ceilometer (BLC), a Vaisala ceilometer, and the Micropulse Lidar (MPL) were used. The BLC and MPL instruments are active, pulse-mode lidars that resolve the height of the cloud base using the return-signal strength. The MPL continuously transmits a 2500-Hz pulse, averages 1 min of observations, and reports the cloud-base height in 300-m bins. Alternatively, the BLC transmits a 1000-Hz pulse for 5 s out of every 30 and averages over the sampling period in 15-m bins. The BLC samples the cloud field incompletely relative to the MPL. Both instruments can detect multiple cloud layers if the pulse is not attenuated. The stochastic model is fairly insensitive to cloud-base height alone. However, determining thickness of the clouds is very important in the stochastic model as it greatly influences how much the incoming solar radiation is attenuated through the volume extinction coefficient. Therefore, the instrument with greater height resolution, the BLC, is preferentially chosen.

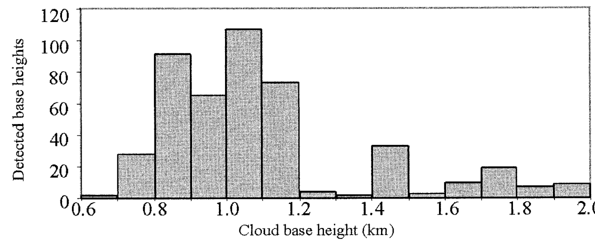

FIG. 3. Cloud-base height distribution.

The cloud-base heights, binned in 100-m increments, are shown for type-1 clouds (Fig. 3). The quantity on the ordinate of Fig. 3 differs from the actual number of clouds present. This will bias the distribution toward larger clouds. The height of a single cloud may be measured more than once as it passes overhead, and the instrument may miss clouds during the processing cycle. The most frequent cloud-base height observed for type-1 clouds is 1100 m. In Planck's 1969 study, the cloud fields were observed to have higher base heights than those measured here. The difference may be explained by differences in near-surface relative humidity between the two locations.

Characteristic cloud-base heights vary significantly among the three cloud types. Type-4 clouds typically have lower base heights than type-1 clouds, while type-8 cloud bases begin higher up. The difference in the characteristic cloud-base height between the three cloud types (Table 2) may be due in part to seasonal variations in the surface forcing. For example, type-8 clouds occur most frequently in April and September, which are the most convective periods at the SGP. Therefore, it is not a surprise that type-8 clouds have notably higher cloud-base heights. The error for reported cloud-base heights is dependent upon which cloud-base detection instrument is used. The minimum error is $\pm$7.5 m, which corresponds to the height resolution of the BLC, and the maximum error is 150 m for the MPL.

It is of interest to note a relationship between cloud-base height and liquid water path (Fig. 4). Although there is large scatter in the data, it appears that there is a general increase of about 65 g m^{-2} for every km increase in cloud-base height. This relationship may indicate deepening of the boundary layer and growth of the cloud thickness during the course of the day. Note that 11 February 1998 and 11 September 1998 do not follow the same trend. It is likely that this is due to seasonal dependence of boundary layer convection.

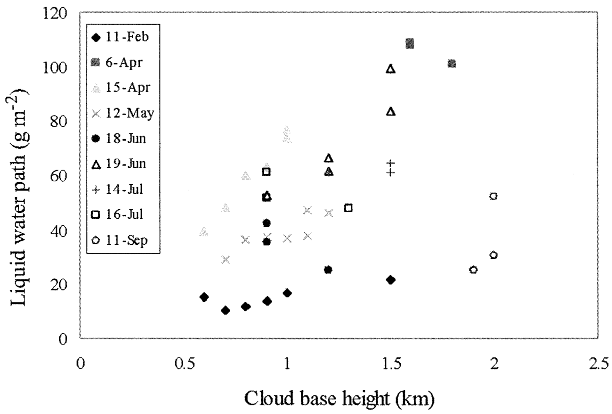

FIG. 4. Scatterplot of cloud-base height vs liquid water path for each hour of observations.

2) Cloud-top height

There are few accurate cloud-top height measurements available for this time period, which will adversely influence the determination of the geometrical cloud thickness. However, there are several approaches that can be considered: using boundary layer top height as a proxy, MPL observations, and climatology. The cloud-top height of type-1 clouds is likely to be limited by the height of the boundary layer top. Therefore, profiles of temperature and relative humidity may be used to approximate the altitude of the cloud top with the altitude of the inversion. Radiosonde data can be used for this purpose, but is available infrequently (2–3 day^{-1}). The sonde height resolution is ~50 m, but is dependent on the ascent rate of the balloon. The cloud-top height as indicated by the available sonde launches is typically ~100–200 m higher than the cloud-base height observed by the BLC.

The 915-MHz radar wind profiler (RWP915) also contains a Radio Acoustic Sounding System (RASS; Wilczak et al. 1996). The RASS measures the virtual temperature profile that can also be used to indicate the cloud-top height. At the SGP site the virtual temperature profile is sampled during the first 5 min of each hour. The average over that time is reported as the hourly average. Analysis of the virtual potential temperature profiles closest in time to the occurrence of the scattered clouds in the study confirms that cloud-top height occurs near the top of the boundary layer for type-1 and type-4 clouds. However, the altitude of the capping inversion occurs at or very near the cloud-base height reported by the BLC. The resolution of the virtual temperature profiles is 110 m, which suggests that type-1 and type-4 clouds may be no more than a few hundred meters thick.

For type-8 clouds, the cloud top is expected to be above the top of the boundary layer. So the approximate technique above is not sufficient. The MPL data include cloud-top height, but the instrument is limited in height resolution as mentioned above and can be inaccurate if the clouds are thick. The MPL indicates that, for type-1 and type-4 clouds, the cloud-top heights occur in the same height bin (within 300 m) as the cloud base. Type-8 clouds have cloud-top heights that range from 300 to 1200 m above the base of the cloud.

Climatological descriptions or prior field studies of marine-based fair-weather cumulus that give an aspect ratio (height to diameter) are used for comparison (Plank 1969; Hozumi et al. 1982). In general, the cloud depths for type-1 clouds are similar in scale to the horizontal dimension (shown below). Therefore, the aspect ratio (cloud height to cloud diameter) is typically about 1. This is consistent with the study by Plank (1969), who determined this value to be 1–2 for fair-weather cumulus populations over Florida, depending on the time of day. However, it is possible that cumuli over land may have different vertical extents than those over water due to different surface forcing and water content of the atmosphere. Clouds that originate from a lower surface-relative humidity will be thinner, because their lifting condensation level is closer to the top of the boundary layer. Plank observed that the cloud size increased during the day as surface heating increased, most notably in vertical extent. It is likely that this value does not reach 2 for type-1 clouds over the Southern Great Plains. Type-4 clouds have an aspect ratio of approximately ½ and type-8 clouds have an aspect ratio of 2–3. This observationally determined aspect ratio is conceptually useful and can be employed when cloud-top height measurements are not available.

3) Cloud fraction

Cloud fraction can be thought of as the amount of cloud occupying a specified space, usually defined as the percentage of a horizontal area covered by cloud. In most, modern cloud–radiation parameterizations cloud fraction is the only input parameter that contains information about the structure of the cloud field. For example, in a plane-parallel model like that used in this study, cloud fraction is used to weight the sum of an overcast and clear-sky radiative transfer calculation. In the stochastic model, the cloud fraction is used to calculate the probabilities that weight the gain and loss terms that represent horizontal photon transport in the radiative transfer equations. As the stochastic model incorporates cloud field geometry in the radiative transfer calculation, it also uses the horizontal fraction defined above in combination with the observed cloud thickness to arrive at a volume fraction of cloud. However, cloud fraction is a simplistic representation of the physical presentation of the presence of cloud, at best.

Cloud fraction is derived from observations at the ARM site using several techniques. Once per hour of daylight, a human observer estimates the fraction of sky covered by cloud and records that in the meteorological logs. Additionally, ceilometers or radiometers determine a one-dimensional fraction by calculating the percentage

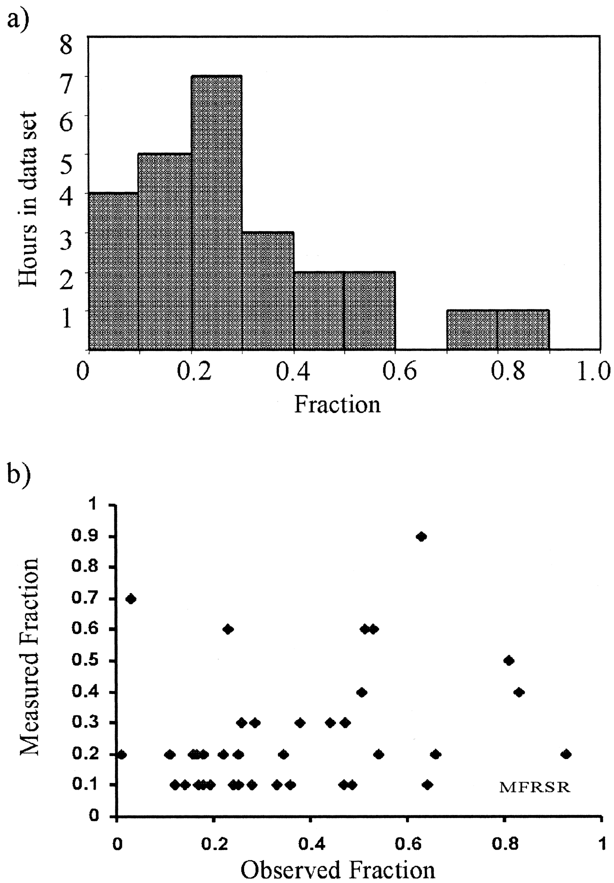

FIG. 5. (a) Cloud-fraction distribution using the MFRSR. (b) Instrumental estimates of cloud fraction vs the human observer's observation.

of time that a cloud was detected relative to the entire time sampled. The MPL provides a more realistic cloud-fraction estimate than the BLC due to more complete temporal sampling.

Hourly averages of MFRSR cloud-fraction measurements are compiled and compared to the human observer reports for each cloud type (Fig. 5). Generally, the human observer reports a greater fraction than that derived from point measurements (Fig. 5b). This supports the results of Bretherton et al. (1995) who observed that human observers often estimate cloud fraction up to 20% higher than the ceilometers. This happens because the observer reports a whole sky fraction, which may include overlapping clouds and cloud sides, while the ceilometer reports a zenith cloud fraction. Neither estimate of cloud fraction may be accurate. The point measurements do not sample the entire field and viewing the cloud sides may skew the human observer's estimate.

In the southern Great Plains, small, scattered cumuli are found to occur most commonly under low cloud-fraction conditions, between 0% and 30%, a value that Plank (1969), Wielicki and Welch (1986), and Hozumi et al. (1982) reported in their studies of fair-weather cumuli. All three cloud types in the current study have been found to occur mostly in this range. In general, changes in cloud fraction noted by the ground observer for a given time interval are also observed in the instrument records. Both models use the cloud fraction derived from the MFRSR observations.

4) Cloud size and spacing

The stochastic approach accounts for the horizontal size and distribution of clouds in the radiative transfer calculation using a characteristic cloud size and spacing (Byrne et al. 1996) that is derivable from observations. In the stochastic model, this information is assumed to be governed by a Markovian probability distribution that is scaled to observations. We present a new technique for estimating the horizontal scale and spacing of clouds from observations to test this assumption. Using a unique combination of measurements, flux data is combined with wind speed and ceilometer-base height to yield horizontal scales as shown below.

The MFRSR (Harrison et al. 1994) is used to calculate how long the direct normal radiation is blocked by a cloud. Multiplying this time by the wind speed at the observed cloud-base height provides a one-dimensional estimate of cloud size. It can be envisioned as if the instrument's narrow field of view ($\sim 8°$) traces a path from the leading edge to the trailing edge of the cloud overhead. To remove instrument noise, the data are normalized by the most proximate clear-day signal, to determine a transmission ratio (Dong et al. 1997). The transmission ratio threshold is chosen to identify cloudy segments of the signal, with an average threshold of 0.9. For consecutive values of 0.9 or less, one cloud length is recorded. Values greater than 0.9 are counted as clear-sky segments. The resulting cloudy- and clear-sky distances are compiled in a population distribution.

The low-sampling rate of the MFRSR (0.05 Hz) limits the detectable cloud size, which will be a function of wind speed. Clouds transiting the viewing area in less than 20 s may not be recorded. Additionally, partial cloud coverage of the field of view may be characterized as total coverage leading to an overestimate of the cloud size by the radius of the viewing area. To limit this effect, the lengths calculated in this analysis are minimum possible sizes. This bias is small, and negligible relative to the undersampling of the cloud field. For clouds that are small enough to pass over the viewing area in 20 s or less, approximately half may be missed. This requires that long time series of data be analyzed. Another consideration in the ability to discern clouds is that the aperture is angular. Therefore, the resolution of this technique varies with height. At a characteristic height of 800 m, the aperture radius is 57 m.

The wind speed measured by the RWP915 (Wilczak et al. 1996; Angevine et al. 1998) at the ARM site is combined with the cloud-base height information to give

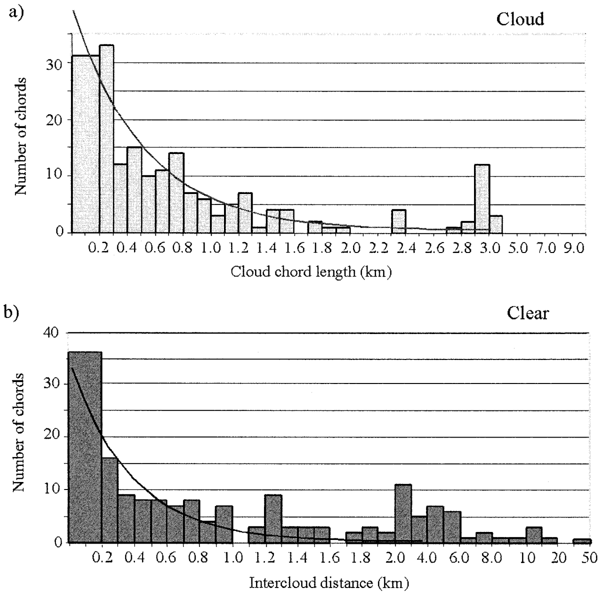

FIG. 6. (a) Cloud-size histogram and (b) cloud-spacing histogram for type-1 clouds. Fits are following Plank (1969).

an indication of the geometrical size of the overhead clouds. The RWP915 measures the backscatter from a transmitted pulse along five pointing directions to obtain a vertical profile every 5 min over the last 50 min of each hour. There are 11–12 profiles averaged each hour. Hourly averages of wind speed are sufficient for conditions where the atmospheric state is not changing rapidly with time. In general, the wind speed at the cloud-base height during the time of interest is between 8 and 10 m s^{-1}, with the exception of the two days in July where the mean wind speed was around 5 m s^{-1}. The wind speed varies no more than 1 m s^{-1} between hours when these scattered cloud fields were present. When possible, the wind speeds from the RWP915 were compared with those measured by radiosondes. They were found to differ by no more than 1 m s^{-1}. The minimum uncertainty in the cloud-size calculation due to the error in the wind speed is ± 40 m.

The cloud segment distributions from the MFRSR are multiplied by the average wind speed at the cloud height on an hourly basis. Cloud sizes are then binned to the nearest 100-m increment, and the cloud-size population distribution is compiled by cloud type and summed over all hours in the dataset. Figure 6a illustrates the resulting cloud-size distribution for type-1 clouds. For convenience, the bins have been combined for cloud sizes greater than 3 km. The most commonly occurring cloud size for fair-weather cumuli is observed in the 200–300-m range. Clouds smaller than this cannot be discerned in the MFRSR signal, and so it is best understood that the most frequently occurring clouds are 300 m in size and smaller. Error introduced by partial cloud coverage in the viewing angle of the MFRSR is 60 m at the most common cloud-base height. The upper limit on the horizontal size of the small clouds is determined by the boundary layer thickness. The largest observed scale for type-1 clouds is approximately 4000 m. This is in agreement with previous studies (Plank 1969; Wielicki and Welch 1986). Integration of the probability distribution completes the conversion from cloud transit time to the horizontal information required by the stochastic model.

Cloud spacing is determined using the same techniques as cloud size. Previous studies have observed that the distance between the clouds is proportional to the cloud size for clouds up to 500 m in effective diameter (Joseph and Cahalan 1990). Therefore, if the clouds are of a detectable size, the spacing between them should also be discernible. The resulting cloud-spacing distribution for type-1 clouds is shown in Fig. 6b. Both distributions have a similar trend, but the maximum in the cloud-spacing distribution is lower than expected ($\leq$200 m). This between-cloud distance is approximately one-half the size of the clouds. This value may be artificially low, as the technique described above cannot distinguish between intercloud distances and cloud holes. Joseph and Cahalan (1990) observed the most frequent spacing between cloud centers to be 500 m, which compares well with this study. For clouds smaller than 1 km in effective radius, Joseph and Cahalan observed the distribution to be independent of spacing.

To better address the limitation of using the above one-dimensional technique to represent a two-dimensional field, an additional analysis was performed. For five days when type-1 clouds occurred, the above analysis was repeated using six MFRSRs distributed over Oklahoma. Two of these radiometers are located at the center of the ARM SGP site, and the other four surround the central two. The smallest distance between the peripheral stations and the central ones is 20 km and the largest is 90 km. The same wind speed and cloud-base height were used for all six stations, assuming that these characteristics were consistent throughout the cloud field. The resulting frequency distributions (Fig. 7) of cloud size and intercloud distance have the same features as in Fig. 6. This result suggests that averaging a single station over long periods yields similar cloud scales to using multiple horizontally distributed observations over shorter times. It is, therefore, possible to obtain robust statistics describing the cloud field from point measurements, given enough time. This type of analysis was also performed with an infrared thermometer, yielding similar statistics.

In Figs. 6 and 7, a fit to the data is overlaid. The line follows Plank's (1969) empirically derived formula $y = \alpha e^{-bD}$, where D is the size of the clouds in the bin, α is the typical number of clouds in the volume, and b is empirically determined. For Fig. 7, the coefficients are indicated on the figure. The curves represent Markovian distributions. The cloud field appears to be appropriate for tests of the stochastic model. The hourly distributions that are compiled to form Fig. 6 are used for the stochastic model input.

The results in Figs. 6 and 7 compare reasonably well with those of Plank (1969), who used aerial photography to determine cloud statistics for cumulus cloud fields present over Florida. Plank (1969) observed that the smallest observable clouds were the most populous, as did Hozumi et al. (1982). Notably, the information about the cloud size and spacing, which is of critical importance to the stochastic model, does not vary much among the three cloud types. The population distributions are virtually indistinguishable.

In addition to the two aircraft studies of cumulus populations by Hozumi et al. (1982) and Plank (1969), high-resolution satellite images have been used to study type-1 clouds. Wielicki and Welch (1986) determined from the analysis of Landsat images of fair-weather cumulus clouds that the shape of the cloud-size population distribution for their results compared favorably with the Hozumi et al. (1982) and Plank (1969) studies. However, Wielicki and Welch (1986) observed more large clouds and fewer small clouds, indicating that the distribution was shifted to slightly larger scales. They state that this difference in the distribution relative to Plank and Hozumi et al. occurs because the individual cells of multicelled clouds were counted as individual clouds in the aerial photograph analysis. The technique presented in this article does not differentiate between cloud cells and individual clouds, and so it is reasonable to expect that the distribution would have a similar shape to those from aircraft studies.

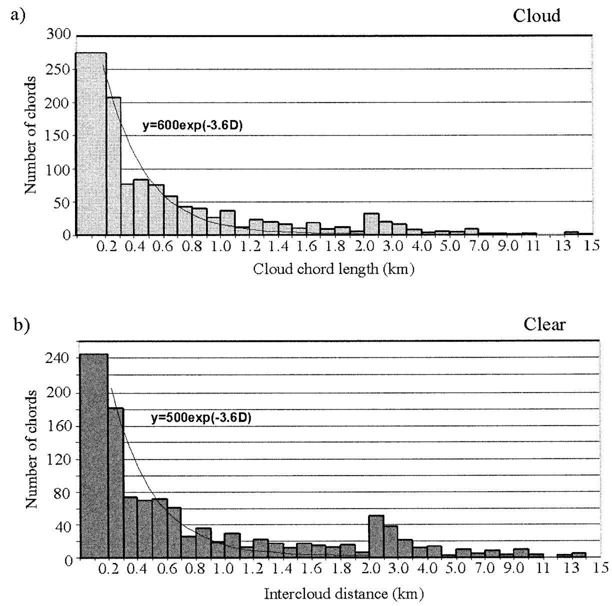

FIG. 7. (a) Cloud-size histogram and (b) cloud-spacing histogram for type-1 clouds using six MFRSRs. Fits are following Plank (1969).

4. Stochastic modeling results

The interest of using observed cloud properties as input to the stochastic model is to gauge the model's ability to represent the influence of actual clouds on the predicted domain-averaged radiation field. Comparisons of the stochastic model with a plane-parallel cloud–radiation model are performed to evaluate the performance of the more realistic code relative to a typical AGCM parameterization. The plane-parallel model ingests the same cloud fraction as the stochastic model on an hourly basis. Additionally, the liquid water path and droplet effective radius input into the stochastic model are used to provide the plane-parallel model with an hourly optical depth using the relation discussed in section 3. Results will be shown for the five days when type-1 clouds were present, and the rest will be discussed.

The input derived from observations for the stochastic model, described in section 2, is ingested hourly for all 16 days in the dataset. For cloud-base and cloud-top height, the peak of the hourly probability distribution functions is input. These values are combined to calculate a cloud thickness that is used in the derivation of the volume extinction coefficient. In the case of cloud fraction and liquid water path, the input values are hourly means. As mentioned previously, droplet effective radius is fixed at a constant value of 6 μm. Cloud horizontal scale is input as a characteristic cloud scale, which is defined as the integration over the probability distribution of horizontal cloud sizes (Malvagi et al. 1993).

For the model runs discussed in this section, profiles for the midlatitudes calculated by McClatchey et al. (1972) are employed in both models. Inputting measured atmospheric profiles alters the model-predicted downwelling shortwave radiation (DWSR) at the surface by no more than 5 W m^{-2}. It is anticipated that the stochastic model will predict less DWSR than the plane-parallel model when the horizontal transport of photons is important. The stochastic model calculates the influence of photons traveling from cloud to cloud, thereby increasing the photon pathlength as well as increasing the likelihood that the photons will be absorbed before reaching the surface. However, in low cloud-fraction situations where the clouds are quite small, the stochastic model may predict more downwelling shortwave radiation at the surface than the plane-parallel model as it is better able to represent the paucity of clouds (small volume extinction coefficient).

As the stochastic model could greatly improve the realism of an AGCM environment, output radiative fluxes are also evaluated using observations. The downwelling shortwave radiation calculated by both models is a domain-average value, and therefore comparison is made to an average over a surface network of hemispheric radiometers that are part of the Oklahoma Mesonet (Brock et al. 1995). The Oklahoma Mesonet is a network of 114 stations spread out over Oklahoma. The shortwave radiometers at each station are broadband

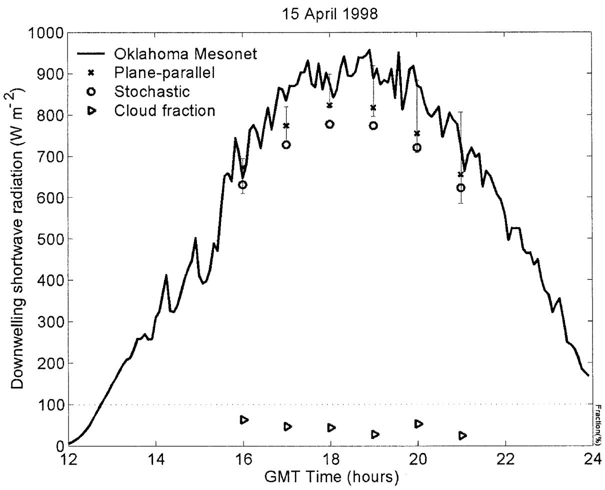

FIG. 8. Model results of downwelling shortwave radiation for 15 Apr 1998 compared with averaged observations from the Oklahoma Mesonet. Cloud-fraction observations are from the MFRSR.

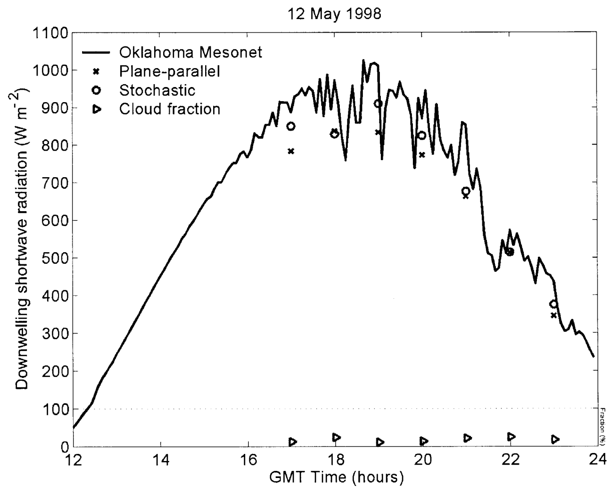

FIG. 9. Model results of downwelling shortwave radiation for 12 May 1998 compared with averaged observations from the Oklahoma Mesonet. Cloud-fraction observations are from the MFRSR.

pyranometers, and the resulting observations are averaged over 5 min. The error in the DWSR at each station is reported to be 5 W m^{-2}, but this error is decreased by averaging over several stations. In the following comparisons, the entire network is not utilized because *GOES-8* satellite images indicate that the broken cloud field often does not cover the entire SGP site. It should be noted that using the entire array of radiometers does not dramatically change the results.

The date 15 April 1998 was chosen from observations as an ''ideal'' day. The characteristics of the cloud field on this day appeared to be closest to the Markovian statistics assumed by the stochastic model for the longest period. The downwelling shortwave radiation observed at the surface and calculated by the two models for 15 April 1998 is shown in Fig. 8. The circles in Fig. 8 represent the stochastic model prediction and the crosses show the results from the plane-parallel model. The triangles indicate the cloud fraction derived from the MFRSR that was input into both models. The differences between the stochastic radiative transfer model and the plane-parallel model are significant. The amount of DWSR reaching the surface in the stochastic model is on average 35 W m^{-2} lower than that calculated by the plane-parallel model. This underestimate is due to a cloud overlap problem between clouds in consecutive vertical layers of the stochastic model. In the plane-parallel model, as in most AGCMs, the cloud thickness is defined as the thickness of the atmospheric model layer. For example, in the plane-parallel model used in this study, the cloud is placed in the second model layer, with a base height of 1.01 km and a maximum thickness of 0.98 km. This constraint is not present in the stochastic model; cloud-base height and cloud-top height are specified independent of model atmosphere vertical structure. However, this may cause the stochastic model to split the cloud field between two consecutive atmospheric model layers. The distribution of clouds between layers is not correlated and so the cloud field is likely to be randomly overlapped in adjacent layers. This will cause the DWSR to be substantially decreased.

The Oklahoma Mesonet data (solid line) have been averaged over 4 of the 114 stations in the network. These four stations are within 90 km of the central facility of the ARM SGP. The cloud field measured at the central facility is assumed to be uniform over the four stations, which is supported by satellite data. Compared to the gridbox-averaged observations from the Oklahoma Mesonet, both models predict too little radiation reaching the surface. This may be due to errors in the microphysical quantities used to calculate optical depth. The sensitivity of both model predictions of DWSR to errors in LWP is shown in Fig. 8. The error bars represent the downwelling shortwave radiation at the surface calculated when the standard deviation of LWP is input into each model. This represents a 10% change in LWP. The plane-parallel model is somewhat sensitive to LWP, with an average change in the prediction of DWSR of 70 W m^{-2}. The stochastic model is not very sensitive to these changes at the small values of cloud LWP reported on this day. The DWSR changed by no more than 3 W m^{-2}. Most of the underestimation of DWSR by the stochastic model is due to the random cloud overlap issue mentioned above. In all hours, the plane-parallel model's prediction is closer to the observed value.

In Fig. 9, the same comparison is made for 12 May 1998. In this case, the stochastic model calculates DWSR that is equivalent or greater than the plane-parallel prediction. This occurs when the cloud fraction is low, but the individual clouds have high LWP. The average difference between the two models is 32 W m^{-2}. In this case, the stochastic model places the entire cloud field in one layer, and so overlap between model layers is not an issue. Both models still underpredict the do-

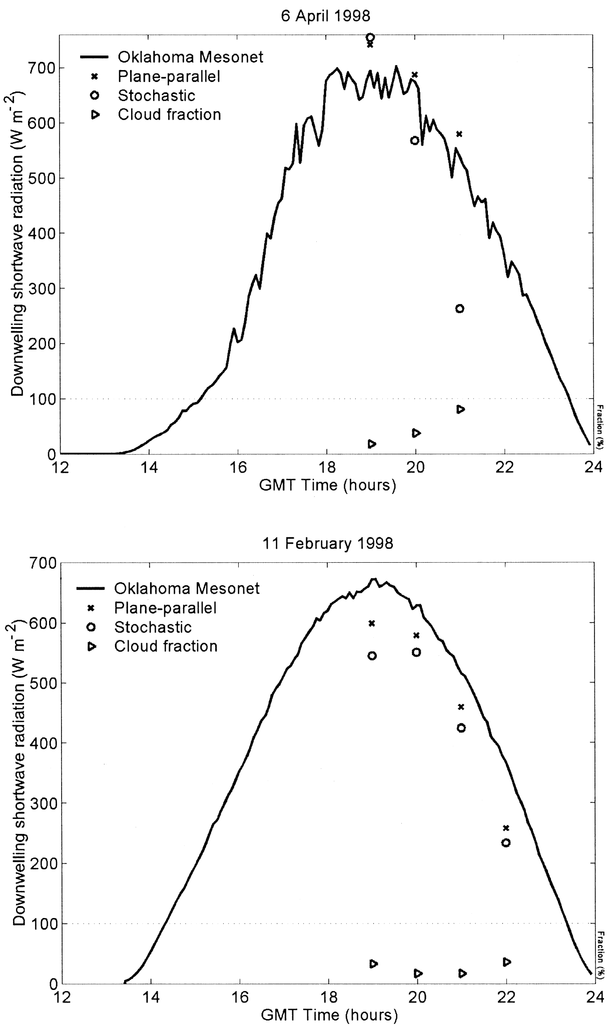

FIG. 10. Model results of downwelling shortwave radiation for (a) 6 Apr and (b) 11 Feb 1998 compared with averaged observations from the Oklahoma Mesonet. Cloud-fraction observations are from the MFRSR.

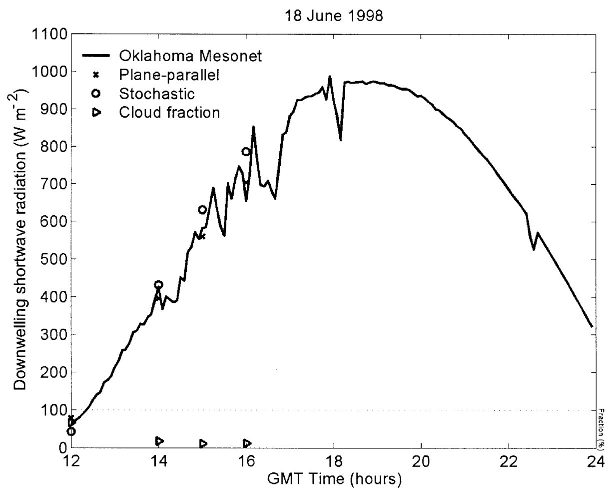

FIG. 11. Model results of downwelling shortwave radiation for 18 Jun 1998 compared with averaged observations from the Oklahoma Mesonet. Cloud-fraction observations are from the MFRSR.

main-averaged DWSR significantly. The stochastic calculation is generally within 50 W m^{-2} of the observed value. Of interest on 12 May 1998 is the difference in the stochastic model simulated values of downwelling shortwave radiation relative to the plane-parallel model between the hours 1700 and 1800 UTC. Further investigation shows that on this day the models agree when cloud fraction is greater than 30%.

Data from 6 April and 11 February 1998 were also used in the modeling study (Fig. 10). At 1900 UTC on 6 April 1998 the models are in fairly good agreement and overpredict the DWSR by 50 W m^{-2} relative to the observations. However, during the last two hours of the comparison on 6 April 1998, the difference between models increases sharply. Analysis of the observational input to the shortwave models indicates that the cloud fraction increases significantly to greater than 80% in hour 21. As cloud fraction increases, the plane-parallel representation of a layer cloud is more appropriate than the random distribution of ellipsoidal clouds used by the stochastic model. This result, combined with that from 12 May 1998, suggests that the stochastic model is only appropriate in certain cloud fields. This supports the result by Byrne et al. (1996) that the stochastic technique will be most useful when the cloud size and spacing are equal to one photon path length, and clouds can act as light sources for each other. The results for 11 February 1998 show the same features as seen in Fig. 8.

Finally, the stochastic model and plane-parallel model predictions of DWSR are compared on 18 June 1998 (Fig. 11). As seen above, the two models disagree most on this day when the cloud fraction is largest. For this day, the observed cloud-base height and cloud thickness were serendipitously close to the predefined plane-parallel model layer values of 1.01 and 0.98 km. This means that the thickness of the clouds is similar in both models, and overlap is not an issue. It is not a surprise that this situation yields the closest agreement between models. The plane-parallel model prediction of DWSR is in very good agreement of the observations, while the stochastic model consistently overpredicts the DWSR by 100 W m^{-2}.

The results shown are representative of the model predictions for the other 11 days in this study. Both models frequently predict less downwelling shortwave radiation reaching the surface than that observed by the four stations of the Oklahoma Mesonet. If the stochastic model places the cloud field in adjacent model layers the DWSR is underpredicted relative to the plane-parallel model. This occurs for all type-8 clouds. In these situations, the discrepancy between the stochastic model and the observations was on average 100 W m^{-2}. Type-4 clouds tend to be quite thin, and so are easily contained in one model layer. In these cases, the stochastic model predicted more downwelling shortwave radiation at the surface than the plane-parallel model, similar to 12 May

1998. Large cloud fractions caused the large errors in the stochastic model. This is probably because the criterion for the scale of the cloudy material being significantly smaller than the domain is not satisfied.

5. Conclusions

Cloud statistics have been compiled for a total of 45 h during 1998 at the ARM SGP site for three cloud types. Data from weather observation logs, cloud observation platforms, and other ground-based instruments are used to determine cloud dimensional and geometric characteristics for each cloud type. The data are analyzed in a manner that provides information that is useful for input to a stochastic radiative transfer model. Results include frequency distributions of cloud-base height, cloud-top height, cloud fraction, liquid water path, cloud horizontal scale, and cloud spacing for each cloud type.

Type-1 clouds, the most frequently occurring clouds in this study, have a characteristic cloud-base height of 1100 m, which is related to the surface forcing present at the time of cloud formation. As demonstrated in earlier studies, these clouds are generally smaller than 500 m in diameter with a fractional sky coverage of 50% or less, which supports the results of earlier studies. Cloud-fraction amounts calculated using instrumental data compare reasonably with amounts reported in the weather observation logs, although there is a low bias consistent with the results of Bretherton et al. (1995). In general, the changes in cloud fraction reported by the ground observer are also seen in the instrument-calculated cloud fraction. Most of the scattered clouds in this study are found to occur most frequently at low cloud-fraction amounts, with the exception of a few hours of type-8 clouds. There appears to be a relationship between liquid water path and cloud-base height that may be useful for parameterization development.

The cloud-scale results show the number of clouds decreases with increasing cloud size. Most clouds in this study have a characteristic horizontal scale of 200–300 m. The maximum observed cloud length is approximately 4000 m. The distribution of intercloud distances has a maximum at $\leq$200 m. The characteristic spacing for type-1 clouds appears to be one-half as large as the characteristic size. This is most likely an artifact of the analysis technique for determining cloud size and spacing. Although the small number of days in this study limits the universality of these results, the robustness of the statistical description of the cloud size and spacing is reinforced by the results calculated using six MFRSR stations over the course of 5 days.

The present study has examined data occurring within only a 1-yr period, and the stringent criteria for selecting the cloud types and times for the dataset significantly decreased the number of hours included in the study. The times selected for study are not evenly distributed over the year, and seasonal variations may account for some of the differences. Therefore, the results should be considered as suggestive of what might be obtained with a larger dataset. Furthermore, this study has considered only low-altitude clouds, although mid- and high-altitude clouds can potentially also be studied by this method. Therefore, we conclude that our method shows promise as a means of obtaining observationally based cloud statistics for input into a stochastic cloud–radiation model.

From the modeling studies it is apparent that the stochastic approximation is sensitive to those input parameters used to calculate a volume extinction coefficient or optical depth. The large uncertainty in the liquid water content can greatly change the output of the plane-parallel model. This will also influence the stochastic model, but will not be significant in low cloud fraction or low liquid water path conditions. In the current stochastic model, the size and spacing between clouds is linked such that smaller clouds are closer together. With many small clouds that are closely spaced, the likelihood of photons becoming extinct in the cloudy layer greatly increases. If cloud fraction increases, without a notable change in the horizontal cloud size, it is more likely that the stochastic model will underestimate the DWSR.

From the initial analysis of ARM data, we demonstrated that it is possible to derive statistical information about the macroscopic features of the cloud field from observations. This information can be ingested by the stochastic model and used in a calculation of radiative transfer through broken clouds. The stochastic approach, while a promising method, indicated sensitivity to several input parameters that describe the geometric features of the cloud field, such as cloud fraction and the cloud horizontal scale. Furthermore, comparison of the stochastic model with a plane-parallel model suggests that both models are sensitive to the microphysical properties of liquid water path and effective radius, which are used to determine optical depth. Improvement in the observations of these quantities will be necessary to fully realize the potential of the stochastic technique.

Acknowledgments. This work was supported in part by the Office of Naval Research under Grant N00014-97-1-0554, by the Department of Energy under Grant DE-FG03-97ER62338, by the National Oceanic and Atmospheric Administration under Grant NA77RJ0453, by the National Aeronautics and Space Administration under Grant NAG5-8292, and by the National Science Foundation under Grants ATM-9612764 and ATM-9814151. This work is based in part on the Ph.D. dissertation of Dana E. Lane (University of California, San Diego, 2000).

REFERENCES

Angevine, W. M., P. S. Bawkin, and K. J. Davis, 1998: Wind profiler and RASS measurements compared with measurements from a 450-m-tall tower. *J. Atmos. Oceanic Technol.,* **15,** 818–825.

Battan, L. J., and C. H. Reitan, 1957: Droplet size measurement in convective clouds. *Artificial Simulation of Rain,* H. K. Weickmann, Ed., Pergamon Press, 184–191.

Benner, B. C., and J. A. Curry, 1998: Characteristics of small tropical cumulus clouds and their impact on the environment. *J. Geophys. Res.,* **103,** 28 753–28 767.

Bretherton, C. S., E. Klinker, A. K. Betts, and J. A. Coakley Jr., 1995: Comparison of ceilometer, satellite, and synoptic measurements of boundary-layer cloudiness and the ECMWF diagnostic cloud parameterization scheme during ASTEX. *J. Atmos. Sci.,* **52,** 2736–2751.

Brock, F. V., K. Crawford, R. Elliott, G. Cuperus, S. Stadler, H. Johnson, and M. Eilts, 1995: The Oklahoma Mesonet: A technical overview. *J. Atmos. Oceanic Technol.,* **12,** 5–19.

Byrne, R. N., R. C. J. Somerville, and B. Subasilar, 1996: Broken-cloud enhancement of solar radiation absorption. *J. Atmos. Sci.,* **53,** 878–886.

Cahalan, R. F., W. Ridgway, W. J. Wiscombe, T. L. Bell, and J. B. Snider, 1994: The albedo of fractal stratocumulus clouds. *J. Atmos. Sci.,* **51,** 2434–2455.

Dong, X., T. P. Ackerman, and E. E. Clothiaux, 1997: Microphysical and radiative properties of boundary layer stratiform clouds deduced from ground-based measurements. *J. Geophys. Res.,* **102,** 23 829–23 843.

Ellingson, R. G., 1982: On the effects of cumulus dimensions on longwave irradiance and heating rate calculations. *J. Atmos. Sci.,* **39,** 886–896.

Fenn, R. W., and Coauthors, 1985: Optical and infrared properties of the atmosphere. *Handbook of Geophysics and the Space Environment,* A. S. Jursa, Ed., Air Force Geophysics Laboratory, 181–188.

Fouquart, Y., and B. Bonnel, 1980: Computation of solar heating of the Earth's atmosphere: A new parameterization. *Beitr. Phys. Atmos.,* **53,** 35–62.

Harrison, L., J. Michalsky, and J. Berndt, 1994: Automated Multifilter Rotating Shadow-band Radiometer: An instrument for optical depth and radiation measurements. *Appl. Opt.,* **33,** 5118–5125.

Houghton, J. T., L. G. Meira Filho, B. A. Callender, N. Harris, A. Kattenberg, and K. Maskell, Eds., 1996: *Climate Change 1995: The Science of Climate Change.* Cambridge University Press, 572 pp.

Hozumi, K., T. Harimaya, and C. Magono, 1982: The size distribution of cumulus clouds as a function of cloud amount. *J. Meteor. Soc. Japan,* **60,** 691–699.

Joseph, J. H., and R. F. Cahalan, 1990: Nearest neighbor spacing of fair weather cumulus clouds. *J. Appl. Meteor.,* **29,** 793–805.

Kite, A., 1987: The albedo of broken cloud fields. *Quart. J. Roy. Meteor. Soc.,* **113,** 517–531.

Kuhn, W. R., 1978: The effects of cloud height, thickness, and overlap on tropospheric terrestrial radiation. *J. Geophys. Res.,* **83,** 1337–1346.

Liou, K.-N., 1992: *Radiation and Cloud Processes in the Atmosphere, Oxford Monogr. Geol. Geophys.,* No. 20, Oxford University Press, 487 pp.

Malvagi, F., and G. C. Pomraning, 1993: Stochastic atmospheric radiative transfer. *Atmos. Oceanic Opt.,* **6,** 610–622.

——, R. N. Byrne, G. C. Pomraning, and R. C. J. Somerville, 1993: Stochastic radiative transfer in a partially cloudy atmosphere. *J. Atmos. Sci.,* **50,** 2146–2158.

McClatchey, R. A., R. W. Fenn, J. E. A. Selby, F. E. Volz, and J. S. Garing, 1972: Optical properties of the atmosphere (3d ed.). Environmental Research Paper 411, Air Force Cambridge Research Laboratories, Bedford, MA, 108 pp.

McKee, T. B., and J. T. Klehr, 1978: Effects of cloud shape of scattered solar radiation. *Mon. Wea. Rev.,* **106,** 399–404.

Plank, V. G., 1969: The size distribution of cumulus clouds in representative Florida populations. *J. Appl. Meteor.,* **8,** 46–67.

Pomraning, G. C., 1991: *Linear Kinetic Theory and Particle Transport in Stochastic Mixtures.* World Scientific, 235 pp.

Senior, C. A., and J. F. B. Mitchell, 1993: Carbon dioxide and climate: The impact of cloud parameterization. *J. Climate,* **6,** 393–418.

Stephens, G. L., 1988: Radiative transfer through arbitrarily shaped optical media. Part I: A general method of solution. *J. Atmos. Sci.,* **45,** 1818–1836.

——, and C. M. R. Platt, 1987: Aircraft observations of the radiative and microphysical properties of stratocumulus and cumulus cloud fields. *J. Climate Appl. Meteor.,* **26,** 1243–1269.

Stokes, G. M., and S. E. Schwartz, 1994: The Atmospheric Radiation Measurement (ARM) Program: Programmatic background and design of the cloud and radiation testbed. *Bull. Amer. Meteor. Soc.,* **75,** 1202–1221.

Stull, R. B., 1991: *An Introduction to Boundary Layer Meteorology.* Kluwer Academic, 666 pp.

Taylor, J. P., and S. J. English, 1995: The retrieval of cloud radiative and microphysical properties using combined near-infrared and microwave radiometry. *Quart. J. Roy. Meteor. Soc.,* **121,** 1083–1112.

Welch, R. M., and B. A. Wielicki, 1984: Stratocumulus cloud field reflected fluxes: The effect of cloud shape. *J. Atmos. Sci.,* **41,** 3085–3103.

Wielicki, B. A., and R. M. Welch, 1986: Cumulus cloud properties derived using Landsat satellite data. *J. Climate Appl. Meteor.,* **25,** 261–276.

Wilczak, J. M., E. E. Gossard, W. D. Neff, and W. L. Eberhard, 1996: Ground-based remote sensing of the atmospheric boundary layer: 25 years of progress. *Bound.-Layer Meteor.,* **78,** 321–349.

World Meteorological Organization, 1956: *International Cloud Atlas.* Vol. 1. WMO, 106–126.